P3HT-fiber-based field-effect transistor: Effect of nano-structure and annealing temperature

Shashi Tiwari[1], Wataru Takashima[2*], S. K. Balasubramanian[1],
Shougo Miyajima[3], Shuichi Nagamatsu[4], Shyam. S. Pandey[3], Rajiv Prakash[5]

[1]Department of Electronics Engineering, Centre for Research in Microelectronics,
Indian Institute of Technology (Banaras Hindu University), Varanasi-221005, INDIA.

[2]Research Center for Advanced Eco-fitting Technology, Kyushu Institute of Technology,
2-4 Hibikino, Wakamatsu-ku, Kitakyushu 808-0196, JAPAN.

[3]Graduate School of Life Science and Systems Engineering, Kyushu Institute of Technology, 2-4 Hibikino, Wakamatsu-ku, Kitakyushu 808-0196, JAPAN.

[4]Department of Computer Science and Electronics, Kyushu Institute of Technology, 680-4 Kawazu, Iizuka, Fukuoka 820-8502, Japan.

[5]School of Materials Science and Technology,
Indian Institute of Technology (Banaras Hindu University), Varanasi-221005, INDIA.

Abstract

poly(3-hexylthiophene)-nanofibers were prepared in ambient conditions and used for the application on organic field-effect transistors (FETs). Top-contact FETs with spin coat and nanofiber-based layers were fabricated to compare their transport performance. It was found that the nanofiber FET show better performance than spin coat one. The annealing effects on the device performance of nanofiber FETs were also investigated from room temperature to 120 ^{o}C. The key performances of the nanofiber FET such as carrier mobility and ON/OFF ratio were improved by the low-temperature annealing up to 80 ^{o}C, which were degraded, however, with higher annealing temperature at 120 ^{o}C. The modulation of surface morphology observed with AFM supports the change of these device performances. Correlation analysis of the mobility, the hysteresis and the OFF current supports the origin to change the FET performances as a

disappearance of nanofiber interspaces and a removal of adsorbed molecules by temperature-controlled annealing.

Keywords: organic field effect transistor, polythiophene, nanofiber, anneal

Introduction

Organic electronics have tremendous benefits over conventional inorganic electronics, such as compatibility with plastic substrates, chemical tunability, mechanical flexibility, facile processability and low cost.[1)] Organic field-effect transistors (OFETs) are very much cost effective and are fabricated to sweep over the complications (high processing costs, requirement of complex fabrication system and costly materials) associated with conventional Si technology.[2)] In the last two decades, OFETs have considerable attraction because of their potential implementation as key-building blocks in display devices, driving circuits, smart cards and low-cost memory devices.[3-5)]

Several conducting polymer based OFETs have been characterized by their outstanding performances and good environmental stability. Improvements in organic nanostructures and device fabrication methods have enhanced OFETs' performances to approach the performances of amorphous silicon based field-effect transistors (FETs). High charge-carrier mobility in OFETs can be obtained by controlling the nanostructure morphology, film uniformity and regular arrangement of organic molecules in active channel thin-film. To fabricate excellent performance exhibiting organic electronic devices, such as photovoltaic devices and OFETs, it is very essential to develop thin-film with high degree of orientation and alignment of polymer molecules, and also controlled morphology of π-conjugate polymers. Such achievements are favorable for efficient charge migration to obtain high performance devices.[3)]

Organic nanostructures such as nanorods, nanobelts, nanowires, nanofibers, nanotubes and nanoribbons have achieved significant progress in fundamental research and their promising implementation in modern organic electronics demonstrates outstanding performances.[6-8)] These organic nanostructures exhibit excellent optical, mechanical and electronics properties due to

their solution processability, mechanical flexibility, electronic tunability, quite fragile and large-scale synthesis.[9] Numerous synthetic and post-synthetic approaches exist for the fabrication of different kinds of organic nanostructures.[10] These nanostructures show very good charge carrier transportation capability due to strong coupling between lower density of structural defects and closely packed molecules. Generally, carrier transportation is very much sensitive to structural defects like molecular disorder and grain boundaries. Therefore, one-directional organic nanostructure is presently considered as an essential structure to enhance the performance of organic devices and circuits because in one-directional nanostructures, carriers can easily and directly move from one point to another point. So, fine aligned nanostructures have promising opportunity in solar cells, light-emitting diodes, FETs, sensors and several microcircuits.[11-13] Nanofibers of organic conjugated molecules have diameter range from 50 nm to 500 nm.

Organic nanofibers and nanowires of conjugate polymers have been prepared by a variety of methods including self-assembly,[14] dip-pen nanolithography,[15] polymerization in nanoporous templates[16,17] and gel-based printing technique.[18] Amongst many organic semiconductors, poly(3-hexylthiophene) (P3HT) is the most extensively studied conducting polymer applicable in organic devices such as sensors, photovoltaic devices, and FETs.[19,20] Usually, thin-films of P3HT prepared with conventional casting method possess many defects and grain boundaries which may degrade the device performance,[21,22] since high performance of a device strongly depends on regular molecular packing and nano- morphology of the polymer.[23] So, plenty of techniques[14-18] have been used to control the growth of polymer micro- and nano-structure morphology. Solution-phase self-assembling of conjugated polymers proposes a strong alternative to thin-film technology.[24-26] P3HT-nanofibers can synthesize through self-assembling and click-coupling of polymer molecules, as stable and uniform suspended nanofibers into

selective organic solvents. The dimensions and density of assembled nanofibers can be controlled by changing the organic solvents and amount of organic materials.[27] P3HT is self-assembled into nanofibers or nanowires in some organic solvents like anisole, toluene, cyclohexanone and p-xylene.[28] Self-assembling of di-block and tri-block copolymers of P3HT with poly(methyl acrylate) or polystyrene can also give well defined nanofibers or nanowires morphology with enhanced electrical conductivity.[29] Recently, one-dimensional P3HT nanofibers exhibit the best OFET device performance amongst the entire reported P3HT based organic field-effect transistors, also.[14]

Nano-structure based dispersion is an alternative form to supply high-performance conjugated polymer as a solution. The self-organization and/or the re-preparation of pi-conjugated polymer nano-structures possibly promote their transport characteristics. For further development of preparation method of nano-structure based dispersions toward high-performance organic electronics, the investigation and characterization of OFET prepared with dispersion is strongly required. In this research, we investigated the transport characteristics of OFET with nanofiber-based P3HT by comparing with the OFET with spin-coat one. Annealing effects on the FET parameters as well as the hysteresis characteristics also discussed for suggesting the mechanism of the modulation of OFF current.

1. Experimental

1.1. Synthesis of P3HT

P3HT was synthesized in the lab. The technique followed in the synthesis of P3HT has been previously reported.[30, 31] 20 ml LiCl/THF was mixed with 5 ml ter-BuMgCl/Et_2O and kept on magnetic stirrer for 5 to 10 min to get a uniform solution. diBromo-3-hexylthiophene (3.261 g)

was added to this solution along with chlorobenzene for increasing the dilution of the solution to prevent precipitation. Further, solution was stirred for 1 h at room temperature. Alfter yellow-color activation of monomer was found after 1 h, Ni(dppp)Cl_2 (54 mg, 1 mol%) dissolved in 2 ml CH_2Cl_2 was injected in the main solution at one time under stirring. 6 h later, the solution was filtered for collecting precipitated parts after the reaction quenched by adding 500 ml methanol (MeOH). Filtrated dark brownish-purple precipitated parts were re-dissolved into chloroform and then re-precipitated with large amount of MeOH, again. The collected cake was washed with acetone by using Soxhlet extraction to remove un-reacted parts and catalyst. The remainder was again treated by Soxhlet extraction with hexane to isolate low molecule part. The remaining-parts were finally extracted with chloroform by Soxhlet extraction to isolate un-dissolved part, dried in vacuum to obtain fine black powder.

1.2. Preparation of nanofiber

A homogeneous dark-orange color solution of 0.1 wt% P3HT was prepared in dehydrated toluene by heating the solution. Then, it was cooled down at room temperature and stored for two weeks at 25 ^{o}C in a temperature controlled chamber. Slowly, P3HT molecules start self-assembled and form stable and uniformly suspended P3HT-nanofibers. As reported by Pron. et.al.,[32] the solubility of P3HT to a certain solvent depends on the molecular weight, thus some high molecular-weight parts are less dissolving even to toluene at room temperature. A very slow precipitation in toluene at room temperature provides a slow aggregation of well-stretched conformational P3HT macromolecules as fiber form. The remaining dissolved parts are, therefore, consisted of a relatively small molecular-weight component. Day by day the color of P3HT solution was changed from dark orange to dark brownish-purple. Detail of the growth of nanofiber and the change in spectra are also reported in the literature.[33, 34] The color change can

be correlated to the quantity of non-dissolved nanofibers in the solution. Fundamental driven force act for the formation of nanofibers is due to π-π interchain stacking.[35)]

Dispersed P3HT nanofibers were separated from its suspension with centrifuging at 6000rpm for 30min. The floating solid parts were collected by decanting and re-dispersed with dehydrated chloroform without drying. Nanofibers in dehydrated chloroform were re-dispersed uniformly by using a cyclo-mixing equipment to get a homogeneous dark-purple color suspension. The concentration of the prepared nanofiber suspension was estimated to be 0.1 wt % calculated by using absorption peak height matching as mentioned the detail in the results. A P3HT dissolved chloroform solution of 0.3 wt% was also prepared for the comparative investigations. The optical properties and surface morphology of P3HT-nanofibers were studied by measuring UV-vis. absorption spectra (JASCO V-750 spectrophotometer) and atomic force microscopy (AFM) (JEOL SPM5200).

1.3. Substrate preparation

A heavily doped silicon wafer (p^+-Si) disc along with thermally grown thin-film (300 nm) of SiO_2 (C_{ox} = 10 nF/cm^2) as gate insulator was cut down into 1 cm×1 cm square chips.[36)] Point dusts from the chips (p^+-Si/SiO_2 substrate) were removed using blower. Now, these substrates were remedied in a mixture solution of distilled water, aqueous ammonia and hydrogen peroxide (ratio 2:1:1 in volume) for 1:30 h at temperature 110 ^oC to make SiO_2 surface hydrophilic (OH group on the surface) and also to remove unwanted organic impurities and dust from the surface of the substrates.[36,37)] After cooling down to room temperature, again these substrates were washed with DI water and dried using blower. Further, the substrates were treated in dehydrated toluene and octyltrichlorosilane (2-3 drops) solution for overnight to get hydrophobic surface of

substrates (p^+-Si/SiO_2). After removing from this solution the substrates were further washed with dehydrated toluene and then treated at 100 ^oC for 15 min to make it dry.

1.4. Device fabrication

Nanofiber suspension was coated over the top of the substrates by using spin coating techniques at room temperature at around 22 ^oC in this study. A 0.3 wt% P3HT/chloroform solution was also coated in order to fabricate spin-coat OFETs for comparison. Spin coat films were prepared with the revolution speed of 3000 rpm for 5 s followed by 5000 rpm for 55 s. The thickness of the films was measured in a range of 45~50 nm by using a DEKTAK 6M Profiler. Through a Ni-shadow mask, two gold electrodes (source/drain) of thickness 40 nm were deposited on the top of the coated thin-films by using thermal vapour deposition method in a vacuum level of 2×10^{-6} torr. Channel length and width of OFET device are 20 μm and 2 mm, respectively. Schematic 3-D structure of OFET is also shown in the inset of Fig. 4(a).

To explore the annealing effect on the FET performances, several nanofiber OFETs were annealed at various temperatures for 10min in an inert condition then cooled down to room temperature. Un-anneald nanofiber OFETs were also fabricated for comparison. All the devices were subsequently moved into a chamber to obtain output and transfer characteristics through a KEITHELY 2612 two channel electrometer at 10^{-6} torr in vacuo.

2. Results and discussion

UV-visible absorption spectrum of a P3HT solution and a nanofiber suspension prepared with chloroform solvent is compared in Fig. 1. It was found that with the absorption peak of P3HT solution at around 450 nm, four other peaks at 470 nm, 520 nm, 560 nm, and 610 nm were

also observed. The vibronic peaks at 520, 560 and 610 nm attributes the absorption of solid-state P3HT. In particular, the relative height of 610 nm is high with a slight narrow full-width at half-maximum, indicating that the solid parts of P3HT should be well-stretched form into a similar manner. These facts suggest the solid part being fiber form. The evolution of these vibronic peaks indicate that suspensions generated with aging the P3HT/toluene solution, however; extension of the conjugate length was due to enhanced π - π stacking of P3HT chains.[38] It should be noted that the suspensions still alive as the solid-state even re-dispersed in the good solvent of chloroform. The formed suspensions suggest being well-ordered/crystallized form with small solubility. Hence, more red-shift and intense absorption were observed as compared to the original P3HT solution. The peak at around 470 nm is associated to the π–π^* transition of individual P3HT molecules as solution part, which is also slightly red-shifted as compared to that for original P3HT solution. This may be because the collected nanofibers are consisted of high molecular weight with having longer π-conjugation length. The long-term fiber formation is a sort of re-crylstallization process, during which a relative low molecular-weight part were failed to solidify. The centrifuging and decanting processes, therefore, remove the dissolved part. Thus, the re-dispersed suspension shows a little longer wavelength. A similar red-shift of the peak also appears in the solution spectra of Fig. 2(a). Finally, we confirmed the solid parts being nanofiber of P3HT by AFM images, which is also discussed later.

For the estimation of the concentration of re-dispers/ed P3HT-nanofiber, we calculated the molar absorption coefficient of P3HT/chloroform solution. Figure 2(b) shows the relationship of the absorption peak height as a function of the concentration. The fine linearity provides the molar absorption coefficient of P3HT solution as the slope of 24 x 10^{-4} $M^{-1}cm^{-1}$. The obtained value is similar to one reported in the literature.[39] Further, from the homogeneous P3HT-

nanofiber suspension used for device coating, one amount was taken to be diluted into 100 times with chloroform, fully-heated till fibers got dissolved completely to obtain as a homogeneous yellow solution. With this solution, one plot between absorption peak intensity at around 470nm in this case was drawn on Fig. 2(b). Using the line fitting parameters obtained in Fig. 2(b), the concentration of P3HT-nanofibers suspension was calculated as about 0.1 wt%. Here, we should concern that the difference in the spectra shape involves a risk for the misestimation of the concentration. But it is enough for clarify the sate in the nanofiber dispersion as a coarse approximation in this study.

The surface morphology of P3HT nanofiber layers and a spin coat film were studied through AFM measurement and the images are shown in Fig. 3. The length and the diameter of nanofibers were observed in the range of approximately 200 to 400 nm and 8 to 10 nm respectively. The surface morphology of P3HT nanofibers still showed their fibrose shape when annealed up to 80 ^{o}C. After annealed at 120 ^{o}C, although a partial area conserved fibrose structure, these fibers were disappeared in other area and particle structure was appeared instead. As shown in the inset, the fundamental shape of these parts is similar to those in spin-coated ones. These findings suggest that the melting temperature of the naofibers in the regime around 120^{o}C in this case. It should be noted that in ref. 40, a low-temperature melting point strongly depends upon the crystallization history. The growth of the nanofibers was found as a long-time phenomenon[41)] and should depend on the molecular weight due to the change in solubility.[32)] These reports support the observed partial conversion of some nanofibers into particles by annealed at 120^{o}C shown in Fig. 3 (c).

Figure 4 (a) shows output characteristics of a nanofiber OFET. The non-linear I_{DS}-V_{DS} curve with pinch-off behaviors represents that the device works as FET. Figure 4 (b) shows transfer

characteristics, representing a normally-on type p-channel behaviors. The field-effect mobility in saturation region, μ_{sat}, and threshold voltage, V_{TH}, were calculated with the transfer characteristics expressed with the equation of:[36)]

$$\sqrt{I_{DS}} = \sqrt{\frac{\mu_{sat} C_{ox} W}{2L}} \left(V_{GS} - V_{TH} \right)$$

where L and W are the length and width of the channel and C_{ox} is the gate capacitance per unit area for insulating layer, respectively. Transfer curves were collected at V_{GS} = –60V in this study. All the calculated device parameters are listed in table 1.

μ_{sat} of an un-annealed nanofiber was found to be seventeen times higher than that of spin-coat film. A larger ON/OFF current ratio was also obtained. There facts conclude that nanofiber OFETs exhibited better performance than that of spin-coat OFET. Furthermore, as already mentioned, the solution concentration to prepare nanofiber layer is about 0.1 wt%, which is smaller than that of 0.3~0.5 wt% as a typical concentration for spin-coating. This indicates that the film preparation with nanofiber suspension is very effective for fabricating OFETs in both means of the device performance and the material usage.

Figure 5 shows the transfer characteristics of nanofiber OFETs with various annealing temperatures. The obtained FET parameters are also listed in Table 1. By a low temperature annealing, charge-carrier mobility and ON/OFF ratio were improved with increasing the annealing temperature up to 80 ^{o}C. The annealing at 120 ^{o}C, however, decreases both of the mobility and the ON/OFF ratio. The deterioration of these device performances are well corresponded to the partial conversion of nanofiber structure into a spin-coat one[35)] as discussed above. These facts suggest that the nano-scale morphology, therefore, significantly affects on the device performance. It is well known that the domain boundary reduces the transport

performance in organic semiconductor films. In the case for the nanofiber based films, each nanofiber is like a domain for carrier transport. The direct bridge of nanofibers between source and drain electrodes provides a ballistic like transport for carriers, which is effective to improve the transport performance. Unfortunately, nanofibers were dispersed uniformly on the channel. Therefore, carriers are transported with parallel, perpendicular and various angled directions of nanofibers. This concludes that the alignment of nanofiber is the next important objective for this research.

Even in a similar morphology annealed at low temperatures, the device performances are sensitive to the annealing temperature between room one to 80 ^{o}C. It should be noted that the hysteresis characteristics in the transfer curves tends to vary with the annealing temperature as found in Fig. 5. Some papers explained this as a presence of impurities.[43)] For more discussion with this phenomenon, the hysteresis intensity, I_{H}, was introduced as the ratio of I_{DS} modulation between the start and the end of the scan of gate voltage for transfer measurement as:

$$I_H = \left(\frac{I_{DS,end} - I_{DS,start}}{I_{DS,start}} \right) \times 100 \quad [\%]$$

The hysteresis is caused by the application of gate voltage as a sort of the high-voltage stress. OFF current is also an important factor for concerning the number of carriers out of control from the gate-voltage. I_{H} and OFF current are plotted for comparison as a function of the annealing temperature in Fig. 6(a). This figure represents that the dependence of both I_{H} and OFF current on annealing temperature are in the same trend as to decrease up to 80 ^{o}C then saturated.

Essentially the switching characteristic of FET is realized by the modulation of carrier number with applying the gate potential as the electrostatic polarization. To sensitize this, the P3HT in the FET channel region should directly contact to the gate-insulator. However, the

P3HT layer consisted of aggregated nanofibers possesses many spaces between fibers. These interspaces provide many parasite nano-scale capacitors and/or adsorption of solvent or water molecules due to imperfect contact of nanofibers on the other ones and on the gate dielectric surface. The existence of the interspaces between nanofibers and gate dielectric decreases an apparent capacitance of C_{ox}, underestimating the mobility and shifting the threshold voltage toward positive. However, the simple existence of parasite capacitance does not provide any hysteresis behaviors.

On the other side, the existence of the interspaces in the channel promotes the adhesion of polar molecules. Under switching the gate-voltage polarity, the adsorbed molecules should rearrange the orientation direction along with the electronic field with a very slow relaxation time. The polarity of dielectric materials strongly affects on the potential distribution. The time-delay of the polarization direction of adsorbed molecules against the gate-voltage sweep is essential to cause the hysteresis on the polarization amount between positive and negative voltage scan. The existence of polar materials in the transport channel also should electro-statistically shield the application of an external electronic-field in these local areas. It is also essential to generate the insensitive carriers against the gate-voltage modulation.

Along with the discussion described above, the population of adsorbed molecules in the interspaces tends to decrease even at a very low-temperature annealing. This supports the monotonic decrease of both the I_H and OFF current at low-temperature zone (Fig. 6(a)). Besides this, the mobility is relatively stationary from room temperature to 40 ^oC annealing, which increased at 60 ^oC and peaked at 80 ^oC annealing (Fig. 6(b)). It should be noted that the nanofibers are very stable in thermal preparation as already described in the preparation process. This suggests that the relative high-temperature annealing in particular near the melting

temperature of nanofiber only promotes the disappearance of the interspaces and the settle down of nanofibers on the gate-dielectric. Then, the diminishing parasite capacitors increase and approach C_{ox} to be 10nF/cm^2 for all the channel areas. As the results, the calculated μ_{sat} should show a maximum.

3. Conclusion

Dispersion of poly(3-hexylthiophene) nanofiber in chloroform were successfully prepared by centrifuging and decanting of precipitated part of toluene solution and used for fabrication of nanofiber-based organic field-effect transistor (FET). The concentration of the re-dispersed nanofiber suspension was examined as 0.1 wt% chloroform solution through UV-vis absorption spectra. Comparison of the surface morphology and the FET performance revealed that the nanofiber morphology was effective to improve the FET performance.

The annealing effects on nanofiber FETs were also studied and concluded that the performance of the devices was increased with elevating the annealing temperature up to 80 ^{o}C, which was, however, deteriorated when annealed at 120^{o}C. The change in surface morphology supports the decrease of the FET performance due to the high-sensitivity of nano-structure on the device performance. The detail analysis of the mobility, the bias-caused hysteresis and the OFF current with annealing temperature represents that the annealing process is also very sensitive to the device performance in nanofiber-based FETs.

Acknowledgements

The authors would like to thank to Department of Science and Technology (DST), New Delhi and Japan Society for the Promotion of Science (JSPS), Japan for the financial support under the DST-JSPS collaborative research work. One of the author, Shashi Tiwari, represents her sincere thanks to Japan Student Service Organization-Short Term Stay (JASSO-SS) for supporting her stay and study in Kyushu Institute of Technology.

References:

1) Y. Sun, Y. Liu, and D. Zhu: J. Mater. Chem. **15** (2005) 53.

2) S.W. Jeong, D.H. Han, and B.E. Park: J. Ceramic Soc. Jpn. **118** (2010) 1094.

3) E. Lim, B.J. Jung, H.K Shim, T. Taguchi, B. Noda, T. Kambayashi, T. Mori, K. Ishikawa, H. Takezoe, and L.M. Do: Org. Electr. **7** (2006) 121.

4) F.Y. Yang, M.Y. Hsu, G.W. Hwang, and K.J. Chang: Org. Electr. **11** (2010) 81.

5) S. Ando, D. Kumaki, J.I. Nishida, H. Tada, Y. Inoue, S. Tokito, and Y. Yamashita: J. Mater. Chem. **17** (2007) 553.

6) L. Jiang, H. Dong, and W. Hu: Soft Mat. **7** (2011) 1615.

7) Y.S. Zhao, H.B. Fu, A.D. Peng, Y. Ma, Q. Liao, and J.N. Yao: Acc. Chem. Res. **43** (2010) 409.

8) H. D. Tran, D. Li, and R. B. Kaner: Adv. Mater. **21** (2009) 1487.

9) B. Su, Y. Wu, and L. Jiang: Chem. Soc. Rev. **41** (2012) 7832.

10) S.B. Jo, W. H. Lee, L. Qiu, and K. Cho: J. Mater. Chem. **22** (2012) 4244.

11) S. Wang, W. Pisula, and K. Mullen: J. Mater. Chem. **22** (2012) 24827.

12) R.S. Friedman, M.C. McAlpine, D.S. Ricketts, D. Ham, and C.M. Lieber, Nature **434** (2005) 1085.

13) F. Qian, S. Gradecak, Y. Li, C.Y. Wen, and C.M. Lieber: Nano Lett. **5** (2005) 2287.

14) J.A. Merlo, and C.D. Frisbie, J. Polym. Sci. Polym. Phys. **41** (2003) 2674.

15) A. Noy, A.E. Miller, J.E. Klare, B.L. Weeks, B.W. Woods, and J. DeYoreo: Nano Lett. **2** (2002) 109.

16) D. Li, and Y. Xia: Adv. Mater. **16** (2004) 1151.

17) P.K. Kahol, and N.J. Pinto, Synth. Met. **140** (2004) 269.

18) H. Kajii, D. Kasama, and Y. Ohmori: Jpn. J. Appl. Phys. **47** (2008) 3152.

19) A. Babel, D. Li, Y. Xia, and S.A. Jenekhe: Macromol. **38** (2005) 4705.

20) T. Pal, M. Arif, S.I Khondaker: Nanotech. **21** (2010) 1.

21) H. Yang, T.J. Shin, Z. Bao, and C.Y. Ryu: J. Polym. Sci., Part B: Polym. Phys. **45** (2007) 1303.

22) S.S Lee, C.S. Kim, E.D. Gomez, B. Purushothaman, M.F. Toney, C. Wang, A. Hexemer, J.E. Anthony, and Y.L. Loo: Adv. Mater. **21** (2009) 3605.

23) Z. Wu, A. Petzold, T. Henze, T.T. Albrecht, R.H. Lohwasser, M. Sommer, M. Thelakkat: Macromol. **43** (2010) 4646.

24) S.J. Park, S.G. Kang, M. Fryd, J.G. Saven, and S.J. Park: J. Am. Chem. Soc. 132 (2010) 9931.

25) E. Lee, B. Hammer, J.K. Kim, Z. Page, T. Emrick, and R.C. Hayward: J. Am. Chem. Soc. **133** (2011) 10390.

26) S.K. Patra, R. Ahmed, G.R. Whittell, D.J. Lunn, E.L. Dunphy, M.A. Winnik, and I. Manners: J. Am. Chem. Soc. **133** (2011) 8842.

27) A.C. Kamps, M. Fryd, and S.J. Park: ACS NANO **6** (2012) 2844.

28) S. Malik, and A.K. Nandi: J. Polym. Sci., Polym. Phys. **40** (2002) 2073.

29) A. Moliton-El, and R.C. Hiorns, Polym. Int. **53** (2004) 1397.

30) M. Jeffries, G. Sauve, R.D. McCullough, Macromolecules 38 (2005) 10346.

31) M.C. Iovu, M. Jeffries-El, E.E. Sheina, J.R. Cooper, R.D. McCullough, Polymer **46** (2005) 8582.

32) M. Trznadel, A. Pron, M. Zagorska, R. Chrzaszcz, and J. Pielichowski: Macromol. **31** (1998) 5051.

33) K. Ashish, W. Takashima, K. Kaneto, and R. Prakash: submitted to J. Polym. Sci. A

34) T. Salim, S. Sun, L.H. Wong, L. Xi, Y.L. Foo, and Y.M. Lam: J. Phys. Chem. C **114** (2010) 9459.

35) J.Y. Chen, C.C. Kuo, C.S. Lai, W.C. Chen, and H.L. Chen: Macromol. **44** (2011) 2883.

36) S. Tiwari, A.K. Singh, L. Joshi, P. Chakrabarti, W. Takashima, K. Kaneto, R. Prakash: Sens. Act. B Chem. **171–172** (2012) 962.

37) K. Kaneto, M. Yano, M. Shibao, T. Morita, and W. Takashima: Jpn. J. Appl. Phys. **46** (2007) 1736.

38) S. Sun, T. Salim, L.H. Wong, Y.L. Foo, F. Boeya, and Y.M. Lam: J. Mater. Chem. **21** (2011) 377.

39) B.W. Boudouris, F. Molins, D.A. Blank, C.D. Frisbe, and M.A Hillmyer: Macromol. **42** (2009) 4118.

40) Y. Zhao, G. Yuan, P. Roche, and M. Leclerc: Polymer **11** (1995) 2211.

41) A. Kumar, W. Takashima, R. Prakash, and K. Kaneto, submitted to J. Mater. Sci.

42) M.M. Torrent, and C. Rovira, Chem. Rev. **111** (2011) 4833.

43) M. Egginger, S. Bauer, R. Schwodiauer, H. Neugebauer, and S.N. Sariciftci, Springer: **140** (2009) 735.

Figure Captions:

Fig. 1. UV-vis. absorption spectra for an original P3HT/chloroform solution and a nanofiber suspension dispersed in chloroform.

Fig. 2. (a) UV-vis. absorption spectra of several P3HT solutions with different concentrations: Blue line shows the UV-vis. absorption spectra of a completely dissolved P3HT-nanofiber/chloroform solution after fully heated. **(b)** Absorption peak height at 450 nm versus P3HT concentration (wt%) line: blue line shows the estimation plot of the dissolved P3HT-nanofiber/chloroform solution, by which the nanofiber concentration can be estimated to be around 0.1wt%.

Fig. 3. AFM images of the nanofiber layer surface **(a)** without annealing, annealed at **(b)** 80 ^{o}C for 10 min, **(c)** 120 ^{o}C for 10 min, and **(d)** the surface of spin-coat film. The scan area dimension is 5 μm×5 μm; inset scan area dimension is 1 μm×1 μm.

Fig. 4. Electrical characteristics of nanofiber OFET: **(a)** Output characteristics. Inset shows schematic 3-D structure of OFET device, and **(b)** Transfer characteristics.

Fig. 5. (a) Transfer characteristics and **(b)** their semi-log plots of OFETs annealed at various temperatures.

Fig. 6 Annealing temperature dependences of **(a)** mobility and ON/OFF ratio, and **(b)** hysteresis Intensity, I_H (%), and OFF current.

Table 1. FET and related parameters of all the OFETs discussed in this study.

Layer preparation	ON current (10^{-5} A)	OFF current (10^{-9}A)	ON/OFF ratio	I_H (%)	V_{TH} (V)	μ_{sat} (10^{-2} cm^2/Vs)
Spin-coat	0.32	28	130	40	35	0.03
Unannealed	1.4	14	1000	33	20	0.52
annealed at 40 ºC	1.6	5.0	3200	16	24	0.53
annealed at 60 ºC	2.8	4.4	6500	9	28	0.59
annealed at 80 ºC	2.4	1.8	13000	6	12	0.80
annealed at 120 ºC	0.27	1.7	1600	5	14	0.18

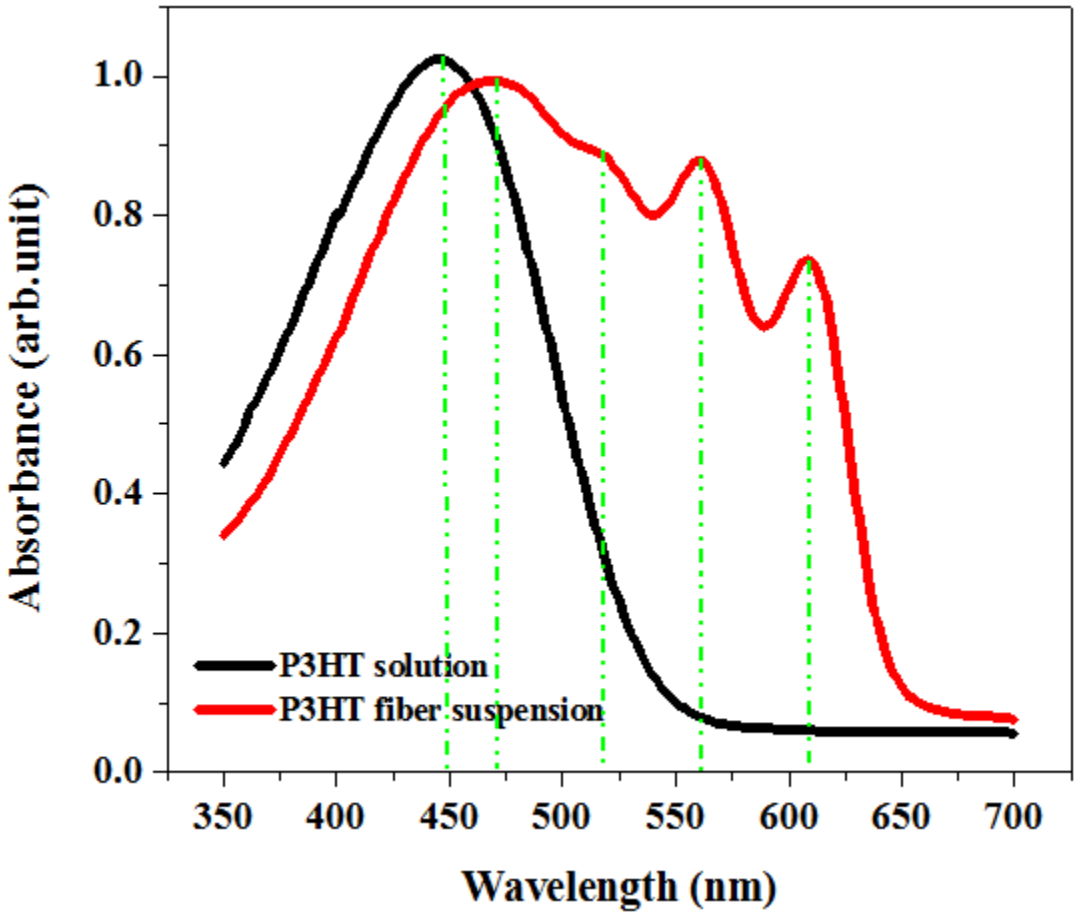

Fig. 1. UV-vis. absorption spectra for an original P3HT/chloroform solution and a nanofiber suspension dispersed in chloroform.

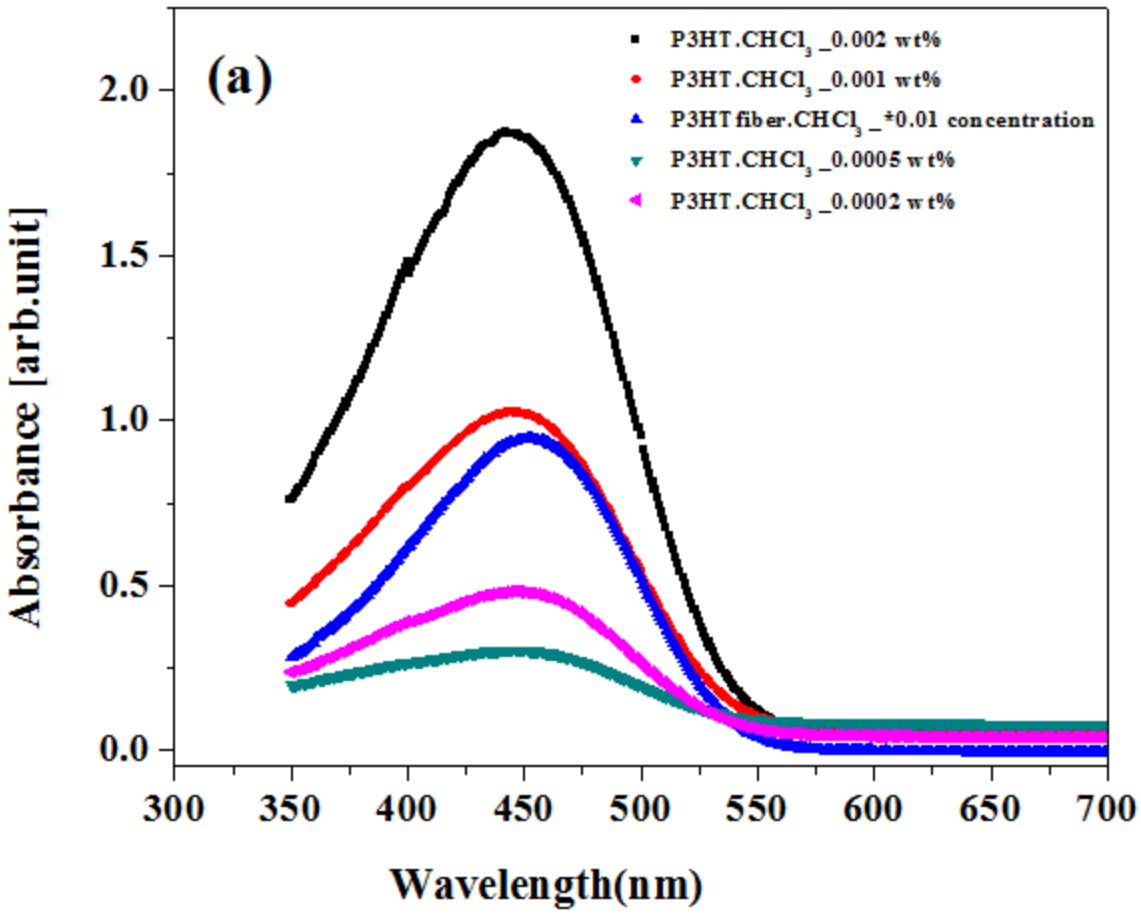
(a)
P3HT.CHCl3 _0.002 wt%
P3HT.CHCl3 _0.001 wt%
P3HTfiber.CHCl3 _*0.01 concentration
P3HT.CHCl3 _0.0005 wt%
P3HT.CHCl3 _0.0002 wt%
Absorbance [arb.unit]
2.0
1.5
1.0
0.5
0.0
300
350
400
450
500
550
600
650
700
Wavelength(nm)

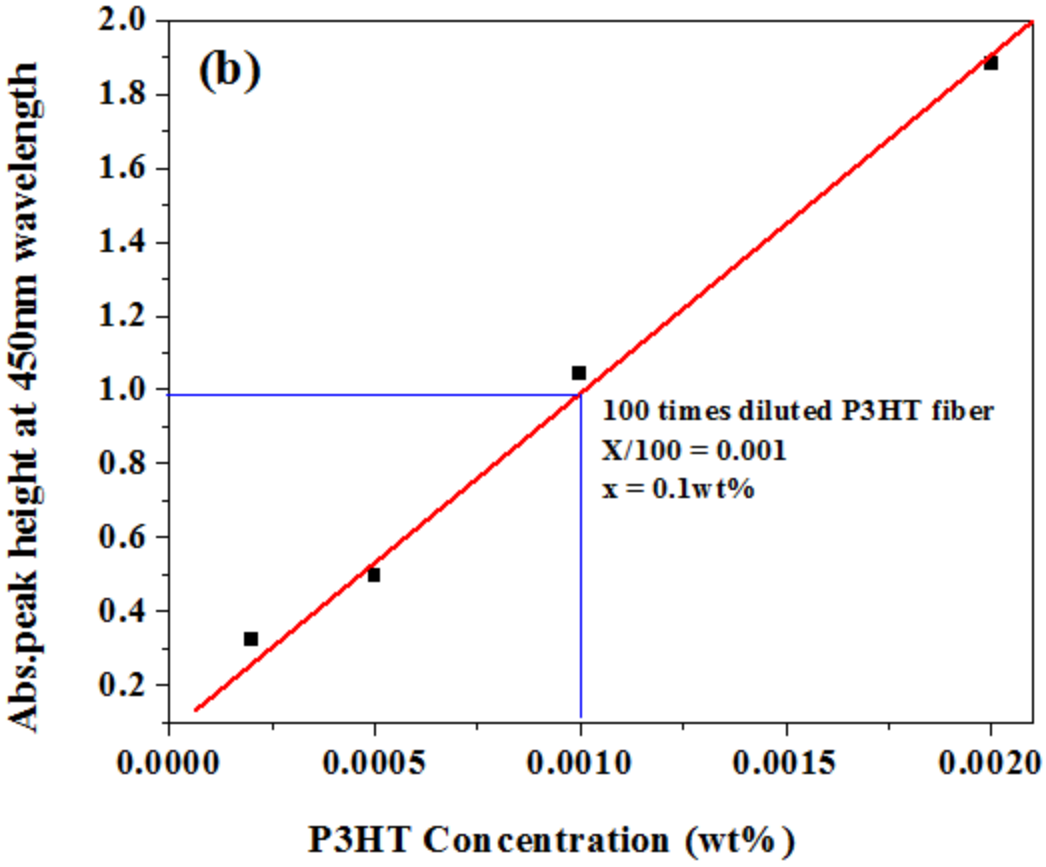

Fig. 2. (a) UV-vis. absorption spectra of several P3HT solutions with different concentrations: Blue line shows the UV-vis. absorption spectra of a completely dissolved P3HT-nanofiber/chloroform solution after fully heated. **(b)** Absorption peak height at 450 nm versus P3HT concentration (wt%) line: Blue line guides the estimation process from the peak height at 470nm of dissolved P3HT-nanofiber/chloroform solution, with which the nanofiber concentration can be estimated to be around 0.1wt%.

.

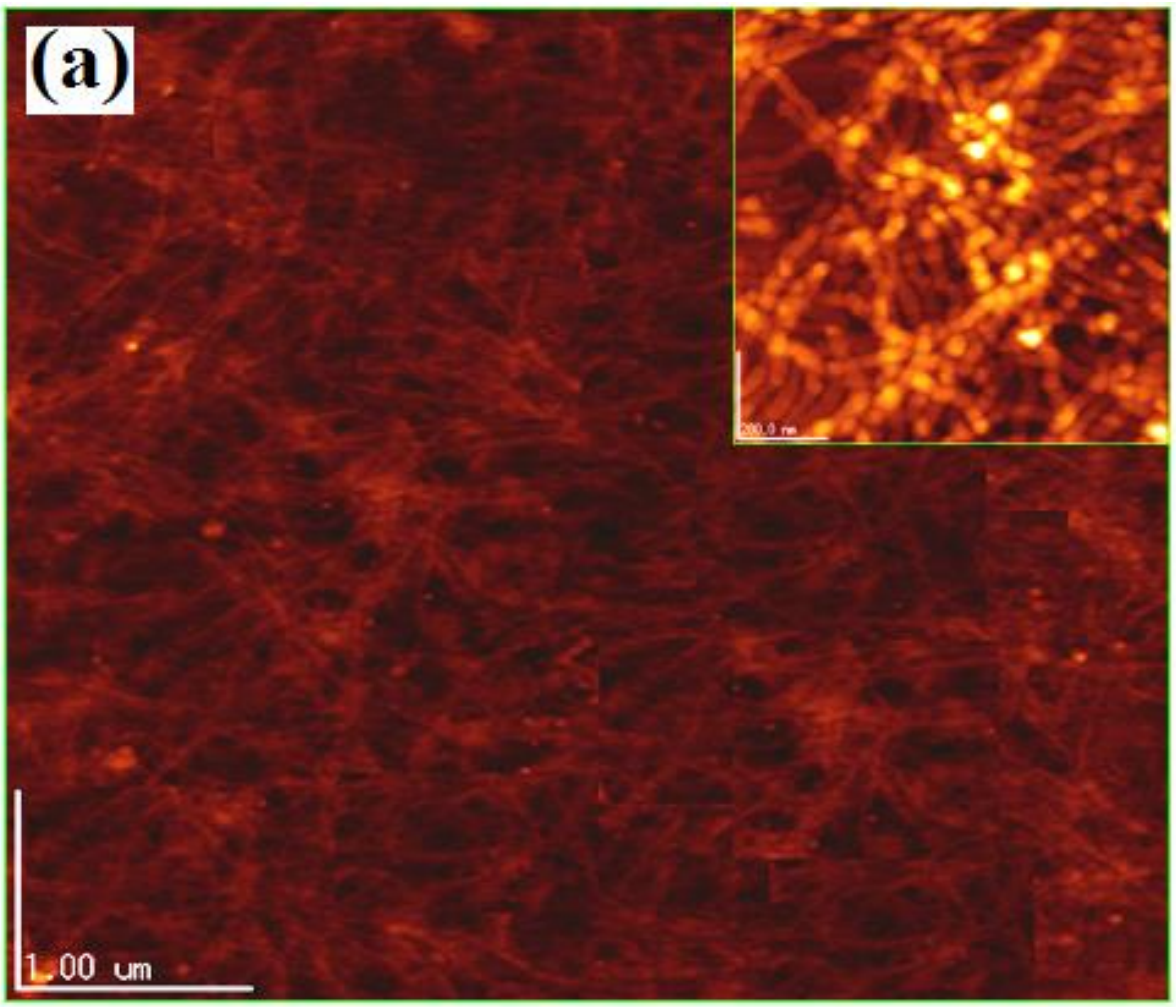
(a)
1.00 um

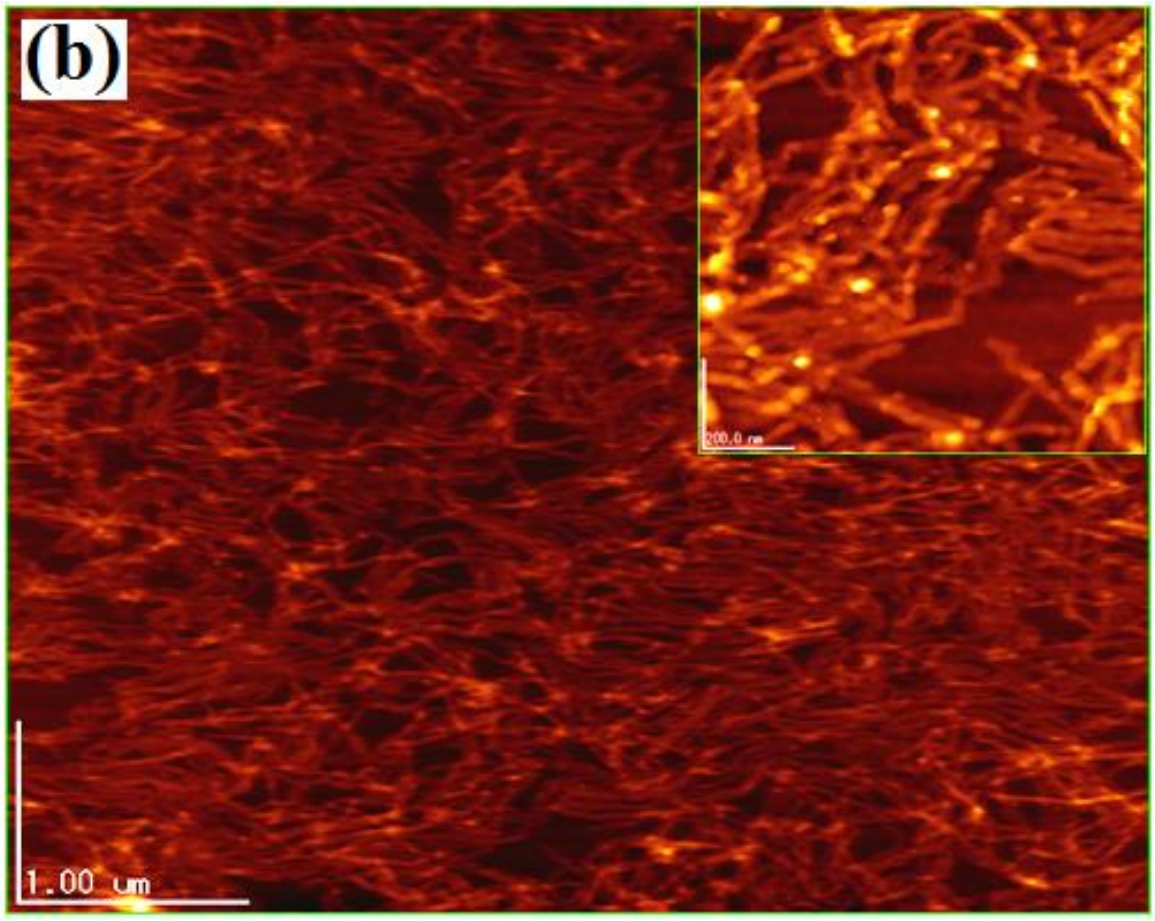
(b)
1.00 um

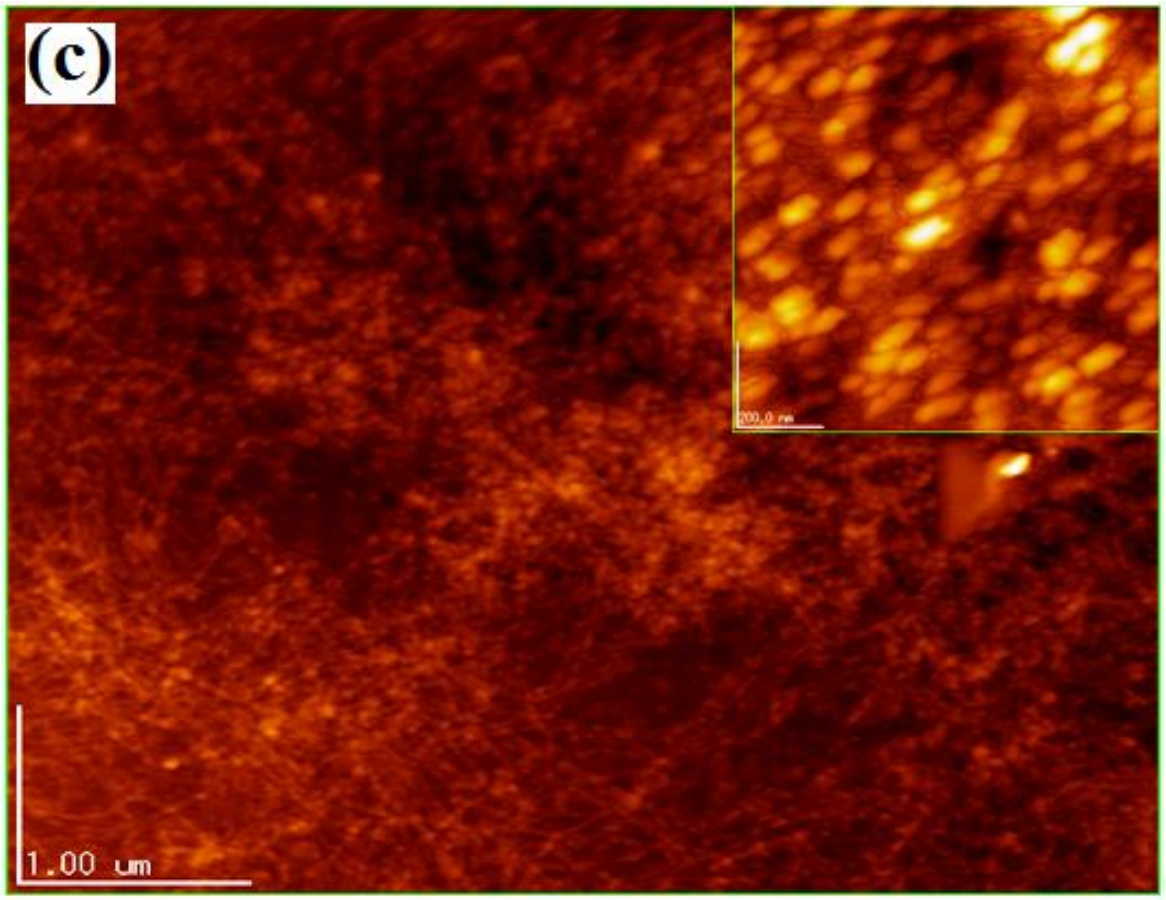
(c)
1.00 um

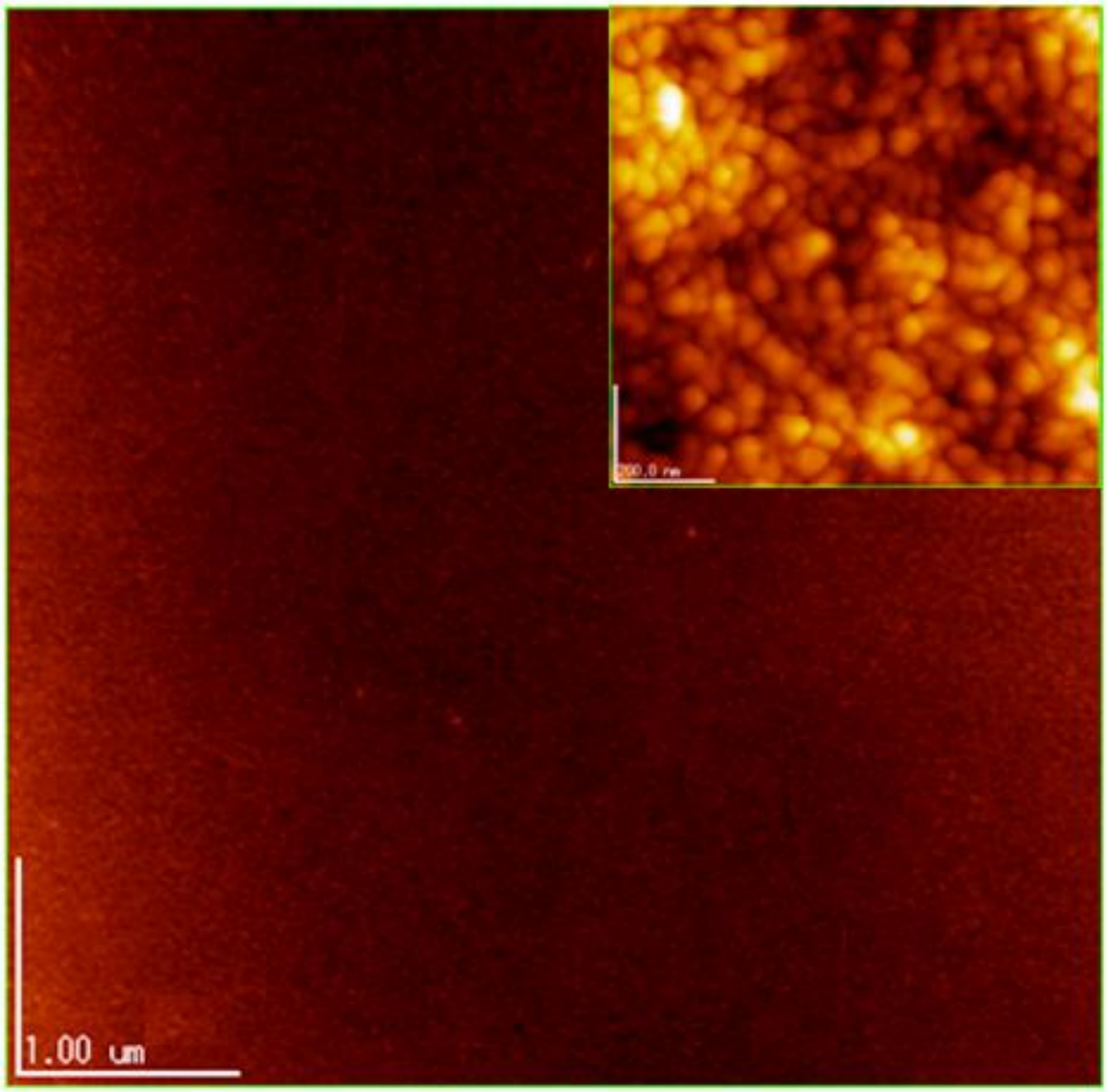

Fig. 3. AFM images of the nanofiber layer surface **(a)** without annealed, annealed at **(b)** 80 °C for 10 min, **(c)** 120 °C for 10 min, and **(d)** the surface of spin-coat film. The scan area dimension is 5 μm×5 μm; inset scan area dimension is 1 μm×1 μm.

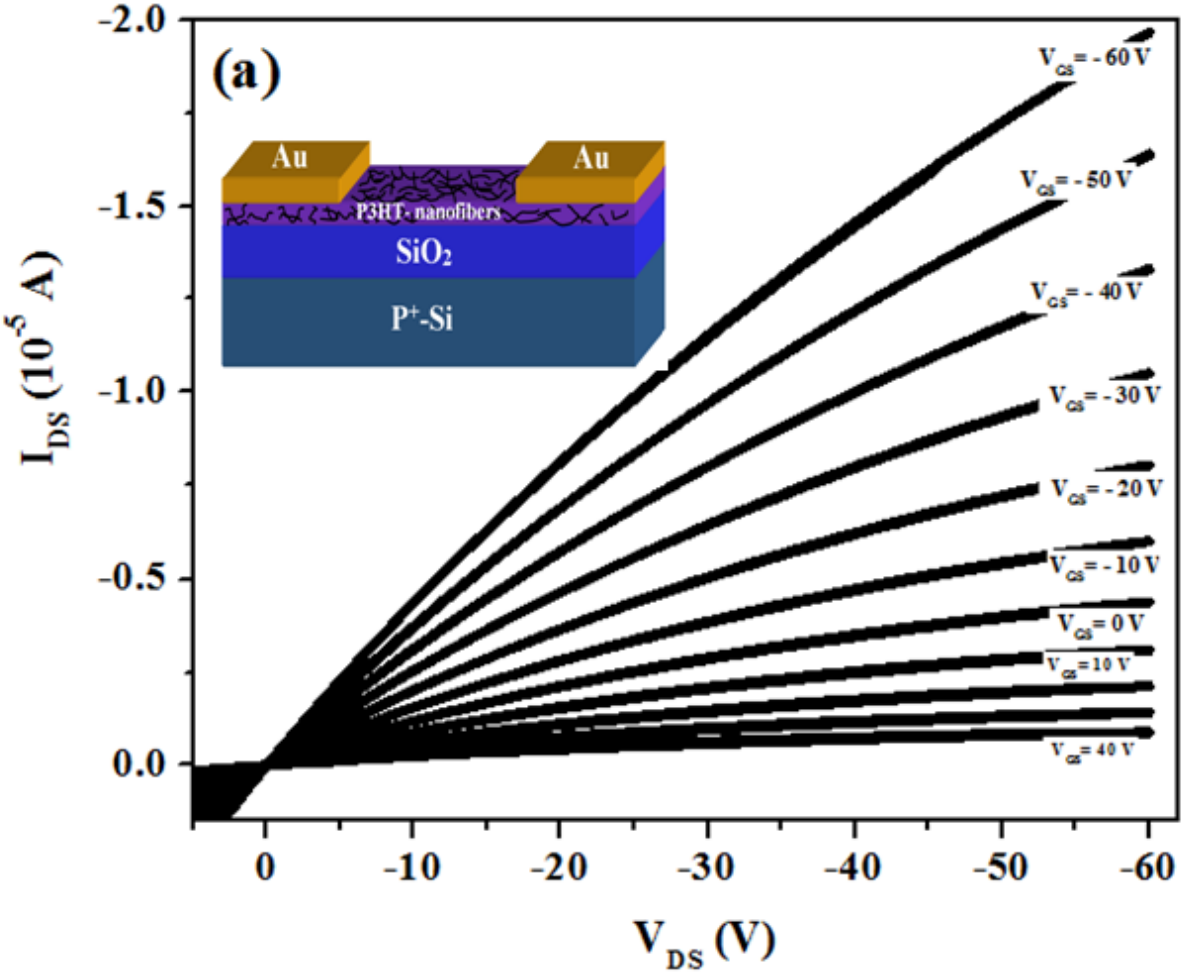
(a)
Au
Au
P3HT- nanofibers
SiO2
P+-Si
V_GS = - 60 V
V_GS = - 50 V
V_GS = - 40 V
V_GS = - 30 V
V_GS = - 20 V
V_GS = - 10 V
V_GS = 0 V
V_GS = 10 V
V_GS = 40 V
-2.0
-1.5
-1.0
-0.5
0.0
I_DS (10^-5 A)
0
-10
-20
-30
-40
-50
-60
V_DS (V)

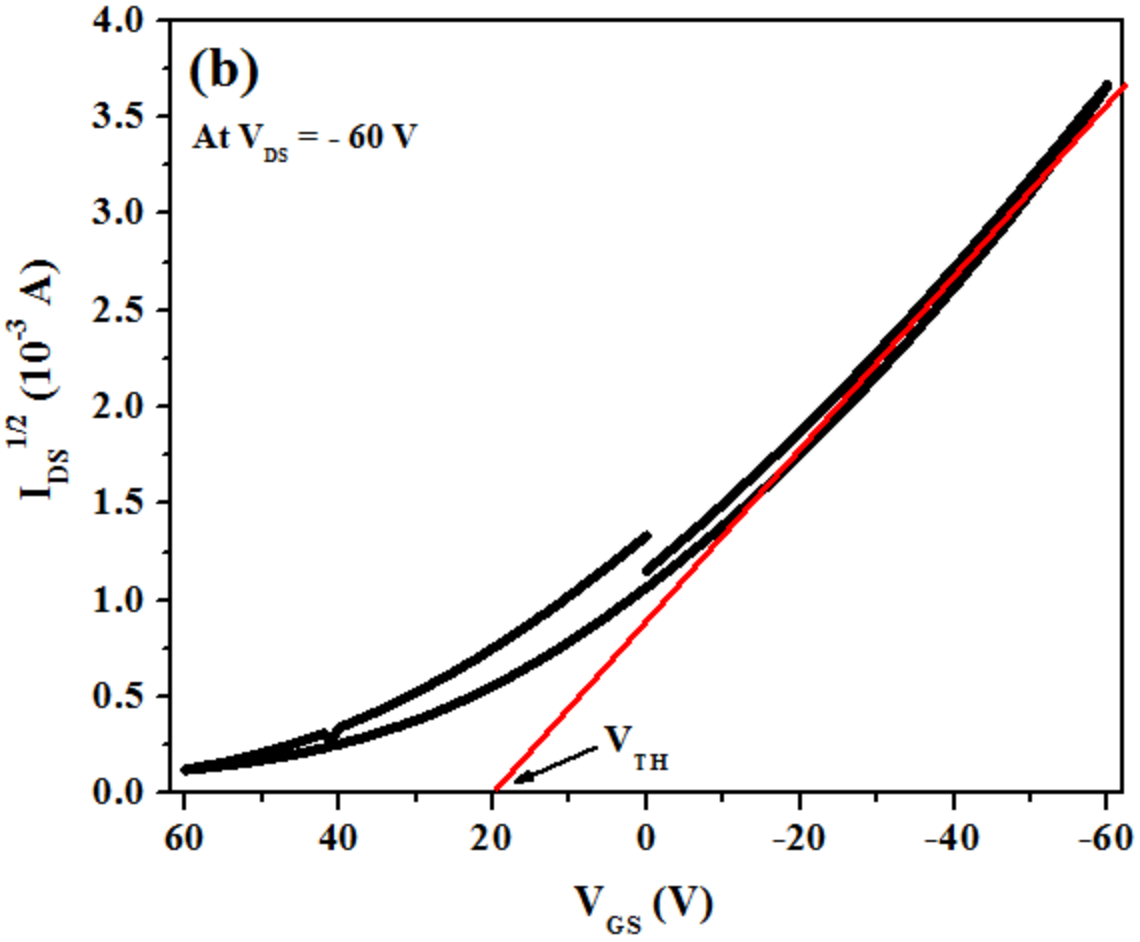

Fig. 4. Electrical characteristics of nanofiber OFET: **(a)** Output characteristics. Inset shows schematic 3-D structure of OFET device, and **(b)** Transfer characteristics.

(a)

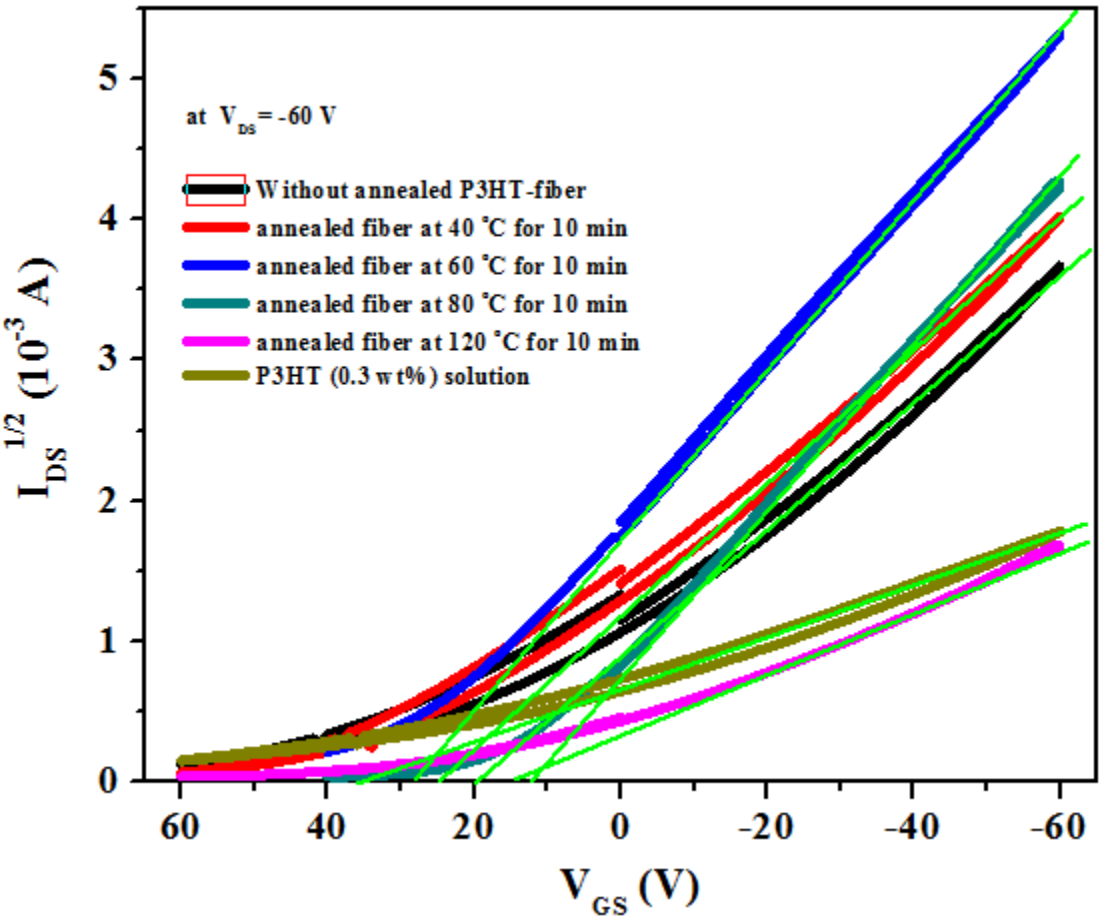
at V_{DS} = -60 V
Without annealed P3HT-fiber
annealed fiber at 40 ˚C for 10 min
annealed fiber at 60 ˚C for 10 min
annealed fiber at 80 ˚C for 10 min
annealed fiber at 120 ˚C for 10 min
P3HT (0.3 wt%) solution
$I_{DS}^{1/2}$ (10^{-3} A)
V_{GS} (V)
5
4
3
2
1
0
60
40
20
0
-20
-40
-60

(b)

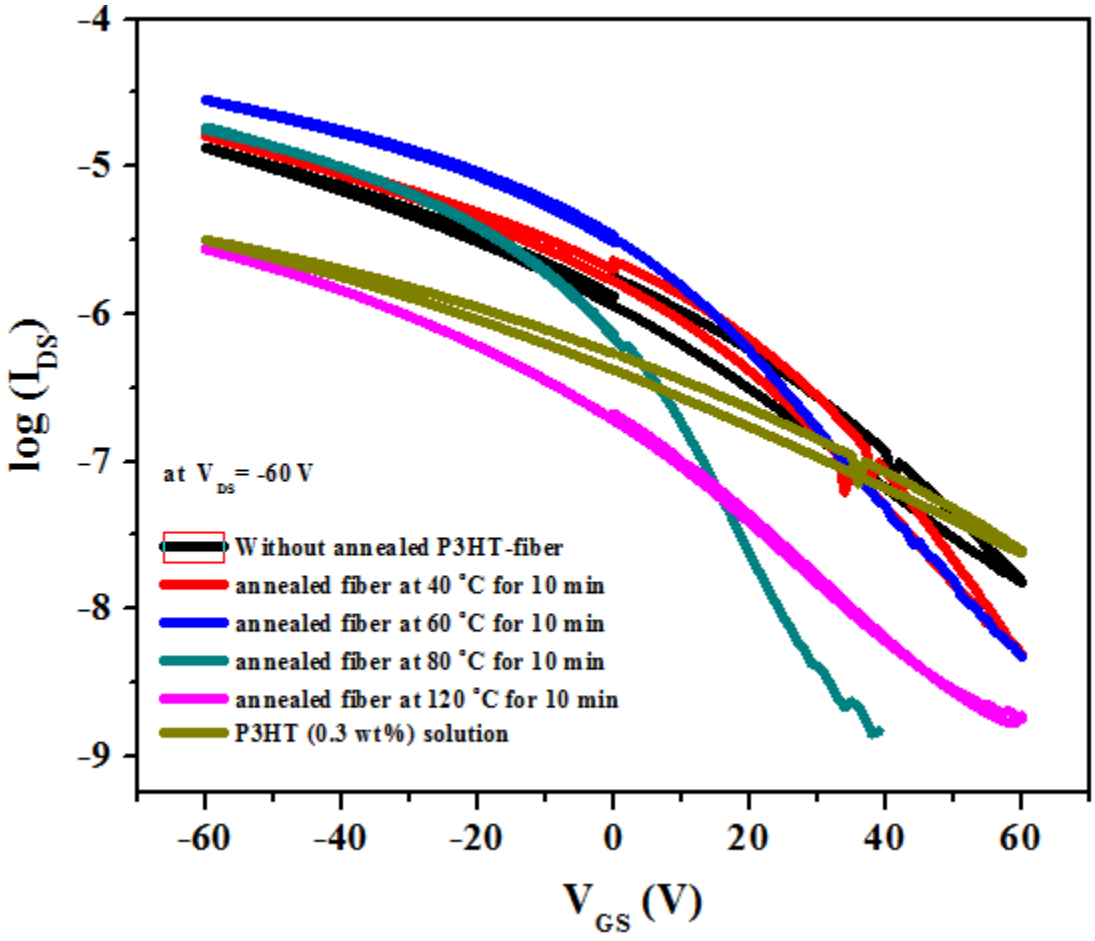

Fig. 5. (a) Transfer characteristics and **(b)** their semi-log plots of OFETs annealed at various temperatures.

(a)

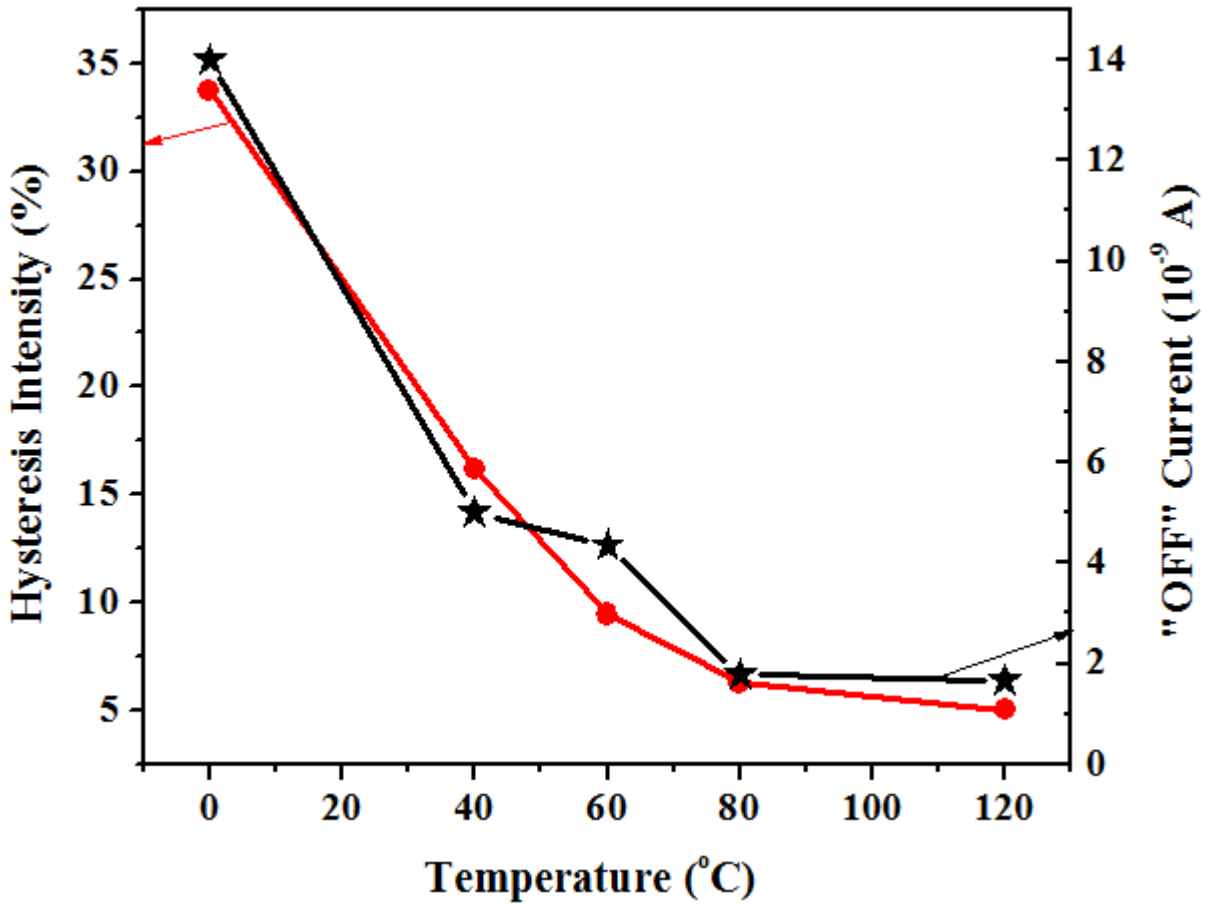
Hysteresis Intensity (%)
"OFF" Current (10^{-9} A)
Temperature (^{o}C)
35
30
25
20
15
10
5
14
12
10
8
6
4
2
0
0
20
40
60
80
100
120

(b)

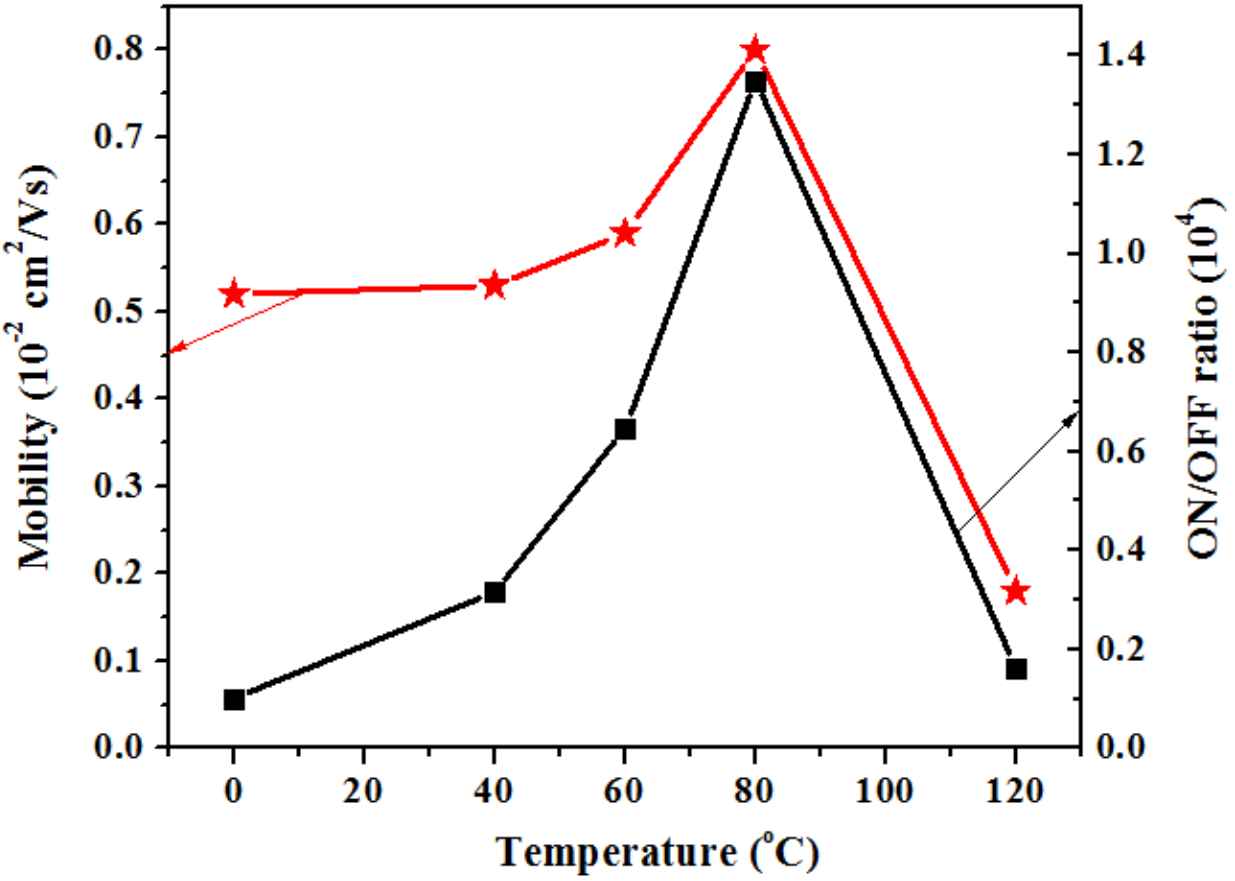

Fig. 6 Annealing temperature dependences of **(a)** I_H (%) and OFF current, and **(b)** μ_{sat} and ON/OFF ratio.